Soil Dynamics and Earthquake Engineering 115 (2018) 66–81

Contents lists available at ScienceDirect

Soil Dynamics and Earthquake Engineering

journal homepage: www.elsevier.com/locate/soildyn

# Removable friction dampers for low-damage steel beam-to-column joints

M. Latour[a], M. D'Aniello[b,*], M. Zimbru[b], G. Rizzano[a], V. Piluso[a], R. Landolfo[b]

[a] Department of Civil Engineering, University of Salerno, Fisciano, Italy
[b] Department of Structures for Engineering and Architecture, University of Naples "Federico II", Via Forno Vecchio 36, 80134 Naples, Italy

ARTICLE INFO

*Keywords:*
Steel beam-to-column joints
Seismic response
Connections
Friction damper
Cyclic tests
Finite element simulations

ABSTRACT

Beam-to-column joints equipped with friction dampers are promising solutions to improve the performance of steel moment resisting frames due to the possibility to guarantee large dissipation capacity limiting the structural damage under severe seismic conditions. In this paper, the experimental tests and the numerical simulations of two types of joints are shown and discussed with the aim of developing pre-qualified configurations. The friction dampers are designed to be easily removable from both the lower beam flange and the column face by means of bolted connections. The devices are composed of a stack of steel plates conceived to assure symmetrical friction. The friction surface is set in vertical direction in first case and in horizontal direction in the second type. The experimental tests confirmed the effectiveness of both examined joints and the finite element analyses allowed characterizing their local response, thus providing additional insights to improve the design requirements.

## 1. Introduction

The design criteria currently implemented by seismic codes are based on the philosophy of hierarchy of resistances, which aims to guarantee overall ductile and dissipative behavior by enforcing the plastic deformation, namely the damage, into specific ductile zones of the structure. However, economic and social reasons have recently pushed researchers and designers towards systems that can resist severe ground motions with low or without structural damage [1].

Traditional seismic resisting systems widely adopted for steel buildings (e.g. moment resisting frames, concentrically and eccentrically braced frames) entail a dissipation mechanism based on plastic deformations of several structural elements, which may correspond large repairing costs in the aftermath of a seismic event. Therefore, the idea of low or free from damage structures has become very appealing in the last decades [2–4].

The use of friction connections is a viable and promising strategy to achieve this objective for steel structures [5–24]. In the framework of Eurocodes, this type of connections can be classified as partial strength according to EN1993:1-8 [25] because their design resistance should be lower than the strength of the connected members to prevent any damage into the primary structural members. EN1998-1 [26] allows the use of partial strength connections provided that their rotation capacity is properly demonstrated. In the case of conventional partial strength joints the ductility can be designed by imposing local hierarchy rules among the components constituting the joints [27–31] and verified by means of pre-qualification tests [32–34].

Moment resisting friction connections are conceived to develop the dissipation mechanism by means of the relative slip into ad-hoc devices located between the lower beam flange and the outer cap plate connected to the column flange, while the upper flange of the beam is connected to a plate either bolted or welded to the column. The cover plate connecting the upper beam flange may be subjected to some moderate plastic bending deformations to accommodate the joint rotation following the sliding of the device, thus enforcing the formation of an ideal center of rotation that prevents the damage of the slab. To increase the moment capacity, friction devices can be also adopted for the beam web. In addition, the resistance of the joint can be modulated keeping the same assembly but varying the friction resistance that changes with the clamping force used for the bolts. Indeed, the friction device is composed of a stack of steel plates that are clamped together by means of tightened high strength bolts, which are inserted in the slotted holes of the plates to allow the relative sliding.

The non-linear response of these connections depends on the type of friction mechanism, which can be either asymmetric or symmetric. The asymmetric friction connection (AFC) has been thoroughly investigated [7–10] and even successfully implemented in recent practice [1]. However, the bolts that clamp the friction pad of AFCs can experience yielding due to large bending moment, shear and axial force interaction, which can induce clamping loss of the bolts and consequently

* Corresponding author.
*E-mail addresses:* mlatour@unisa.it (M. Latour), mdaniel@unina.it (M. D'Aniello), mariana.zimbru@unina.it (M. Zimbru), g.rizzano@unisa.it (G. Rizzano), v.piluso@unisa.it (V. Piluso), landolfo@unina.it (R. Landolfo).

https://doi.org/10.1016/j.soildyn.2018.08.002
Received 10 May 2018; Received in revised form 19 July 2018; Accepted 2 August 2018

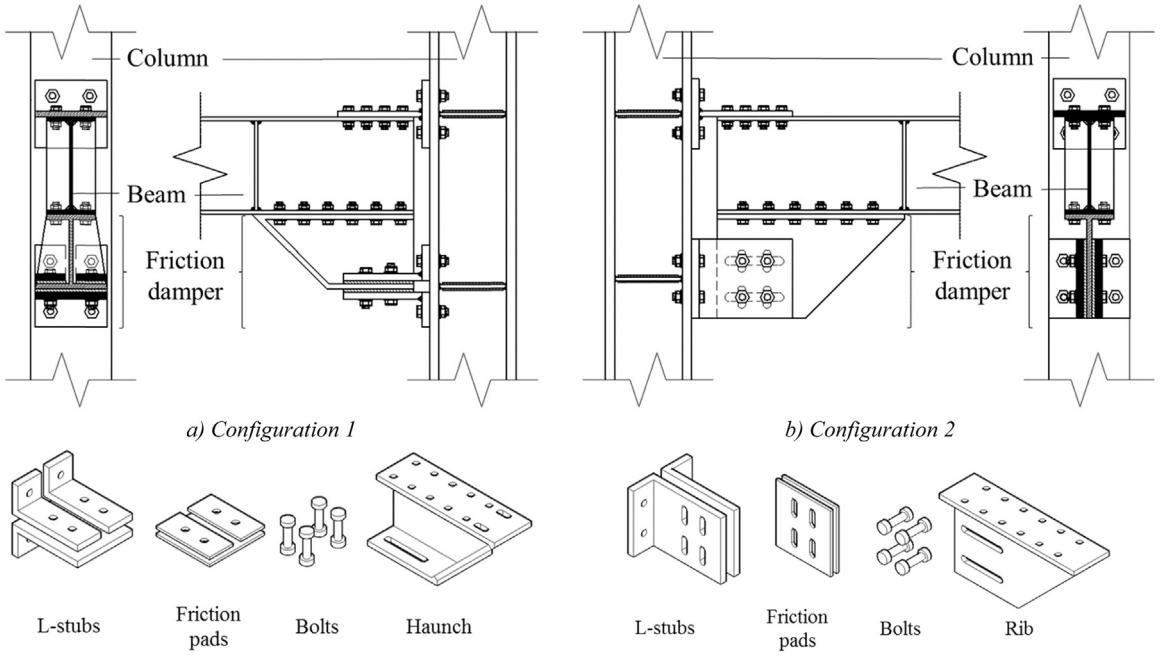


**Fig. 1.** Typologies and features of the investigated joint configurations.

pinching and loss of strength of the connections. On the contrary, these phenomena can be mitigated with the use of a symmetric friction connection (SFC) [16–22].

Latour et al. [23] recently carried out an experimental study on SFCs with the friction damper applied by means of an additional haunch welded to the lower flange of the beam. The friction pad was located at the interface between the haunch and L-stubs that are connected to the column flange. It was composed by an 8 mm S275JR steel plate (steel hardness 211HBW, sand blasted surface) coated with a thin layer of sprayed aluminum to improve the friction resistance with low cost of the raw material, as also shown by [35]. The tests showed that this solution is very effective, because the allowable flexural strength of the connection at column face is greater than the plastic resistance of the connected beam. Hence, full-strength connections can be also obtained without requiring any damage to the beam. In addition, the use of a haunch increases the stiffness of the connection, since its internal lever arm is larger than the beam cross section depth, thus obtaining rigid connections prior the sliding of the device. These features are very important from design point of view, because the structural models adopted for the seismic analysis do not need to account for the deformability of the joints.

It is also worth noting that the geometry of these connections is similar with a split tee connection with the particularity of the friction pads needed in order to ensure specific friction properties. The resistance of the connection is dictated by the friction damper but, once the design resistance is established, the design of such connection can be carried out entirely according to EC3 Part 1–8 [25]. In addition, the constructional costs for such connection are marginally different compared to traditional steel bolted connections. The economic advantages of the MRFs equipped with friction connections include also the limited extent of the damage that is localized at the level of the joint components, this further simplifying the rehabilitation work in the earthquake aftermath [15,16].

However, after severe seismic events the friction pad should be substituted, and the surface of the haunch should be treated to restore its initial roughness and to remove the residual portions of the friction layer scraped out the pad. These types of interventions can arise some operational difficulties especially concerning the tightening of the bolts that clamp the friction device. Indeed, as shown by [21,23] it is crucial to control and guarantee the level of bolt pre-loading to ensure the design value of friction resistance. Indeed, if the clamping force is excessively large, the corresponding strength of the connection can be larger than the resistance of the adjacent members. On the contrary, lower preloading may either anticipate the sliding of the connections under serviceability non-seismic loading or weaken the global structural capacity under the design earthquake that may induce disproportionate rotation demand of the connections.

A viable solution to solve these issues can be the use of removable friction dampers that can be easily detached from both the lower beam flange and the column face by means of bolted connections, thus simplifying the reparability of the friction device. Indeed, if the whole friction damper is conceived as a demountable kit containing both the friction pad and the relevant steel supports, this option allows tightening the bolts in the shop with the reliable control of the applied torque. In addition, the friction kit can be entirely substituted in the aftermath of severe earthquake without the need to perform superficial treatments of the beam flange on site.

These considerations motivated the research activity presented in this paper, which was devoted at developing two types of connections with detachable friction dampers. To achieve this objective both experimental cyclic tests and finite element simulations have been carried out. The paper is organized in three main parts as follows: i) the design criteria of the proposed joints are presented in the first part; ii) the experimental campaign is described in the second part; iii) the finite element simulations and the characterization of the local response of the joints are discussed in the third part.

## 2. Design criteria of joints

### 2.1. Features of the investigated joints with removable friction dampers

The examined joints are characterized by double split-T connections, where the bottom tee element is replaced by detachable friction dampers, as depicted in Fig. 1. The main mechanical difference of the two investigated types of devices is the direction of the friction plan that is horizontal in the case of bolted haunch (hereinafter also

identified as "configuration 1") in Fig. 1a, and vertical in the case of the bolted rib plate (hereinafter also identified as "configuration 2") in Fig. 1b. In both cases the friction pads are made of stainless steel covered by a special type of coating selected based on former studies carried out at University of Salerno [19,20].

The friction kit of the configuration 1 is made of four main components (see Fig. 1c), namely the L-stubs, the friction pads, the preloadable grade 10.9 HV bolts and the removable haunch, which is detailed with slotted holes on the lower side to facilitate the sliding at the interface with the friction pad, while clearance fit bolts are considered for the upper part of the haunch to prevent relative its sliding as respect to the lower beam flange. The L-stubs are welded built-up and have the role of (i) transferring the bolt forces, (ii) clamping together the friction pads and the haunch, and (iii) connecting the assembly to the column flange.

The friction damper of configuration 2 (see Fig. 1d) has vertical sliding surfaces. Hence, to allow the relative slip both the mobile part (i.e. the rib plate) and the fixed parts (i.e. L-stubs and friction pads) are detailed with slotted holes.

### 2.2. Design criteria of the friction connections

The moment resistance of the friction connections ($M_{slip,Rd}$) is assumed equal to the design moment at column face ($M_{Ed}$), which can be set equal to either the value obtained from the structural analysis under seismic condition ($M_{Ed,E}$) or the factored resistance of the beam cross section ($M_{pl,b,Rd}$) projected at column face and scaled down by the factor $\Omega_\mu$ that accounts for the expected overstrength developable by the friction device in order to avoid damage in the beam at the haunch/rib tip. In the first case the beam-to-column assembly should have moment resistance larger than the moment induced by non-seismic loads at ultimate limit state of non-seismic conditions and it behave as rigid-partial strength joint, while rigid-full strength in the second case. In this study the specimens were designed according to the second approach in order to exploit the maximum resistance of the assembly.

Generally speaking, whichever is the design option, set as $M_{Ed}$ the design bending moment of the connection, the required slip resistance of the device can be obtained as follows:

$$F_{slip,req} = \frac{M_{Ed}}{h_t} \tag{1}$$

Where $h_t$ is the lever arm of the connection, namely the distance between the center of rotation and the axis of sliding.

In the present study, in order to exploit the larger flexural strength of the connection keeping elastic the spanning beam, the design moment demand of the connection was set equal to the factored plastic resistance of the beam projected at column face, namely as following:

$$M_{Ed} = (M_{pl,b,Rd} + S_h \times V_h)$$
$$V_h = (2M_{pl,b,Rd}/L_h + V_{Ed,G}) \tag{2}$$

Where $S_h$ is the distance from the tip of the haunch/rib plate to the column face and, being $L_h$ the free span length of the beam from tip to tip of the haunches and $V_{Ed,G}$ is the shear force due to gravity loads. In the cases of the experimental specimens of this study $V_{Ed,G}$ was set equal to zero.

The number of friction interfaces ($n_s$), the mechanical features of the characteristic dynamic friction material ($\mu_{dyn,5\%}$), the number ($n_b$) of bolts and their diameter ($d$) were fixed a-priori. Subsequently, by imposing that the effective slip force $F_{slip,eff}$ has to be larger or equal to the required value (see *Eq.* 1) it can be easily determine the necessary level of bolt preloading ($N_b$) as follows:

$$F_{slip,Rd} = \mu_{dyn,5\%} \cdot n_s \cdot n_b \cdot N_b \geq F_{slip,req} \rightarrow N_b \geq \frac{F_{slip,req}}{\mu_{dyn,5\%} \cdot n_s \cdot n_b} \tag{3}$$

In order to limit the relaxation of pre-loading due to creep phenomena and to prevent the yielding of the bolt shank under bending, on the basis of previous experimental studies [21,35] the optimal values of the clamping force should range within 30–60% of preloading force $F_{p,C}$ recommended by EN1993:1-8 [25]. The design values for $N_b$ are given in Table 5 while the friction material properties are given in Table 7.

The non-yielding components of the joints are designed according to EN1993:1-8 [25] to resist the slip force and the associated moment magnified by the overstrength factor $\Omega_\mu$, which is defined as follows:

$$\Omega_\mu = \frac{\mu_{st.95\%}}{\mu_{dyn.5\%}} \cdot \frac{N_{b.95\%}}{N_{b.5\%}} = 1.97 \simeq 2.0 \tag{4}$$

Where $\mu_{dyn,5\%}$, $N_{b,5\%}$ are the lower-bound values of the dynamic friction coefficient and tightening force, respectively; $\mu_{st,95\%}$, $N_{b,95\%}$ are the upper-bound values of the static friction coefficient and tightening force, respectively. The values of both static and dynamic friction coefficients as well as the tightening forces were derived on the basis of previous experimental studies [18–21,35,45] which addressed aspects related to the friction properties of the coating material and the covered surfaces, the preloading level, creep phenomena, loss of preloading and high velocity load application. On the basis of these studies, the selected friction material is assumed to have predictable and stable friction properties under very severe cumulated displacement histories. However, further studies should be carried out to investigate any aging deterioration along the design life.

Another important check that should be considered is the shear resistance of both the T-stub and L-Stubs at column face. The shear resistance of these connections is evaluated according to EN1993 1-8 [25], while the design shear force $V_{Ed}$ is given by *Eq.* (5):

$$V_{Ed} = \frac{2 \cdot M_{CD}}{L}$$
$$M_{CD} = \Omega_\mu M_{Ed} \tag{5}$$

Where it can be noted that the design shear force is estimated as the ratio between twice the expected strength of the friction joint ($M_{CD}$) and the distance between the column face connections ($L$). In addition, both the T-stub and the L-stubs connections have to be checked to resist the full value of $V_{Ed}$,.

The explanations and the relevant evidence of this recommendation are given hereinafter in Section 4.2.

## 3. Experimental campaign

### 3.1. Test setup

The experimental campaign consisted of 4 tests on friction joints that were performed in the laboratory of the Department of Civil Engineering at University of Salerno.

The test setup is shown in Fig. 2. The columns were pinned in the bending plane of the joint with a cylindrical hinge at one end and a roller at the opposite tip. The beam was laterally restrained by means of a braced frame to prevent its lateral-torsional buckling. Two MTS 243 actuators were used for the tests. The top actuator (load capacity of ± 250 kN and stroke range equal to ± 500 mm) was used to apply the displacement history at the beam tip that was set according to loading protocol recommended by AISC341 [36]. The second actuator (load capacity of ± 1000 kN and stroke range equal to ± 125 mm) was used to apply a constant compression force equal to 30% of the column squash load that was kept constant throughout the duration of each test.

### 3.2. Investigated joints and monitored parameters

As previously discussed, two types of friction dampers were investigated, and their main geometrical features are depicted in

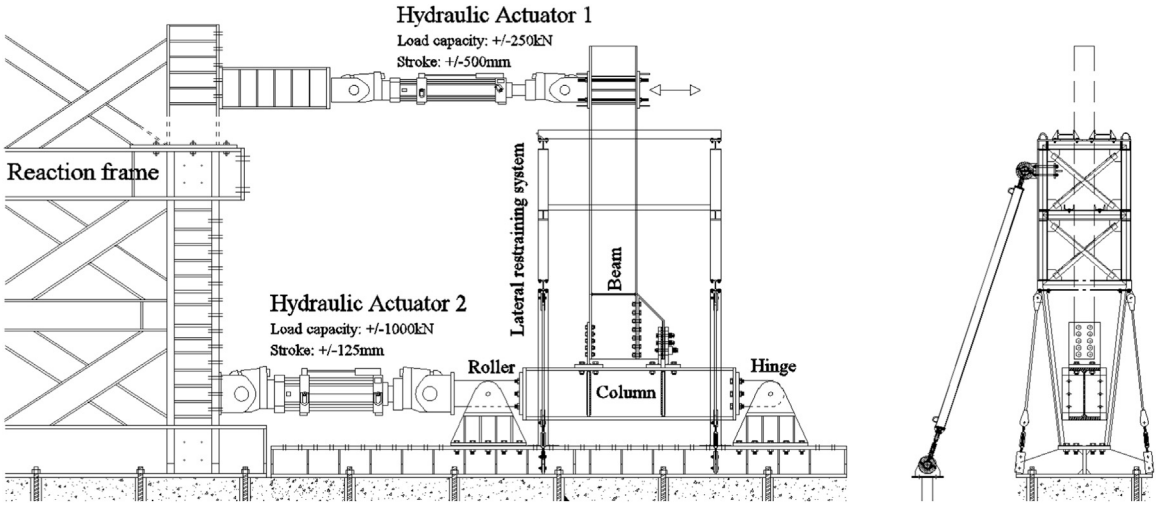


**Fig. 2.** Experimental setup.

Fig. 3a–g. In addition, two beam-column assemblies per joint type were tested to cover the cases of both small (beam IPE270 – column HE 220M) and large (beam IPE450 – column HE 500B) scale structures. In all tested joints the bolts of the friction devices were equipped with special type of disc springs (DS) washers to limit the loss of preloading under cumulated slip, which are non-flat washer with a slight conical shape and are commonly used to solve vibration, thermal expansion, relaxation and bolt creep problems. The DS were stacked both in parallel and in series to increase the strength and the deformability, respectively as shown in Fig. 3. This arrangement was established on the basis of the findings of a former experimental campaign on lap-shear connections [18,19,35]. In addition, preloadable HV bolts [37] were adopted to clamp the friction surfaces.

The overall geometrical features of the tested beam-to-column assemblies are depicted in Fig. 3 and the corresponding values are also reported in Tables 1–5. A label code is used to identify each assembly as follows: 'FD' stands for Friction Device, the first number is related to the joint configuration (1 or 2) and the second number refers the size of the assembly (1 for small or 2 for large). The additional term "DS" identified the use of disc springs. As example, FD-1-1-DS corresponds to the small assembly equipped with the device configuration 1 (i.e. horizontal friction surface) and disc springs.

Both global and local response parameters were monitored during the tests. At global level, the displacements at the tip of the beam and the relevant reaction forces of both actuators were measured (see Fig. 4a). Namely, the bending moment in column axis was evaluated based on the reaction force in the actuator ($F$) and the corresponding lever arm ($L$ – the distance between the actuator and the column axis). The displacement ($u$) at level of the actuator applying the displacement history is used to obtain the chord rotation ($\theta_{chord}$) by dividing it with $L$.

Regarding the local response parameters, the relative displacements (δ) among the components of the connections were monitored by means of LVDTs and the forces into the bolts were measured throughout the experiments by means of torsional loading cells. The relative sliding of the friction damper with respect to the fixed parts (L-stubs) were measured by means of the LVDT-07 (for the configuration 1) and LVDT-02 and LVDT-07 (for the configuration 2), as depicted in Fig. 5. The obtained values were used to evaluate the friction damper rotation ($\theta_{device}$), which is obtained by dividing the displacement $\delta$ with the connection lever arm $z$ measured from the mid-thickness of the T-stub web to the geometrical center of the friction device as detailed in Fig. 4. In addition, LVDT-03 was used to evaluate the opening of the cap Tee stub connection, while LVDT-04 (for the configuration 1) and LVDT-05 (for the configuration 2) were used to monitor the gap opening of the lower L-stub connections.

### 3.3. Test results

All performed tests showed an overall satisfactory response with stable hysteretic behavior and similar features, as depicted in Fig. 6. Indeed, both types of connections performed as rigid up to the static friction resistance of the devices. Following the activation of the sliding, a loss of strength was observed but negligible stick-slip phenomena were observed under load reversal. Both friction assemblies lead to an asymmetric response of the joint, however the difference between the sagging and hogging resistance is larger in the case of the configuration 1 (i.e. horizontal friction surface), which also experienced the more pronounced degradation of the cyclic resistance, especially for the large assembly FD-1-2-DS.

The different flexural resistance experienced under sagging and hogging can be explained by analyzing the local deformation demand in the upper T-Stub (which connects the top flange of the beam to the column) and the lower L-Stubs (which connect the device to the column). The upper Tee was the same at the same beam-column assembly of both joint types, thus the differences can be explained by considering the different deformability of the L-Stub arrangements that differ with the friction connection configurations. As depicted in Fig. 7, the deformation of the Tee has values in the same ranges for the 2 pairs of tested joint assemblies i.e. the small assemblies (i.e. FD-1-1-DS and FD-2-1-DS) and the large assemblies (i.e. FD-1-2-DS and FD-2-2-DS) present T-stub flange opening of maximum 0.5 mm and 1.0 mm, respectively. On the other hand, Fig. 8 shows that the L-stub flange opening is substantially larger in the joint assemblies detailed with the horizontal friction damper configuration (i.e. FD-1-1-DS and FD-1–2-DS) than the values measured for the joints with the vertical damper (i.e. FD-2–1-DS and FD-2–2-DS). It is worth noting that the difference is terms of gap opening corresponds to the difference in terms of flexural strength under sagging loading.

In line with the findings of a previous numerical study carried out by the Authors [38], the difference between sagging and hogging bending resistance for the first configuration can vary up to the 25%, while the second configuration has a lower difference (about 15%).

As shown in Fig. 6, the larger beam-column assemblies exhibited the larger degradation of the strength for increasing levels of rotation. This performance was caused by two effects: first, the use of longer bolts (with the same diameter of those used for smaller specimens) and secondly, the bolt clamping was higher (see Table 6 that reports the average tightening forces measured per specimen). The former feature induced more flexibility in the bolts, which corresponded larger bending demand in the shank as well as rotation of head and nut a consequential reduction in clamping force that translates into a

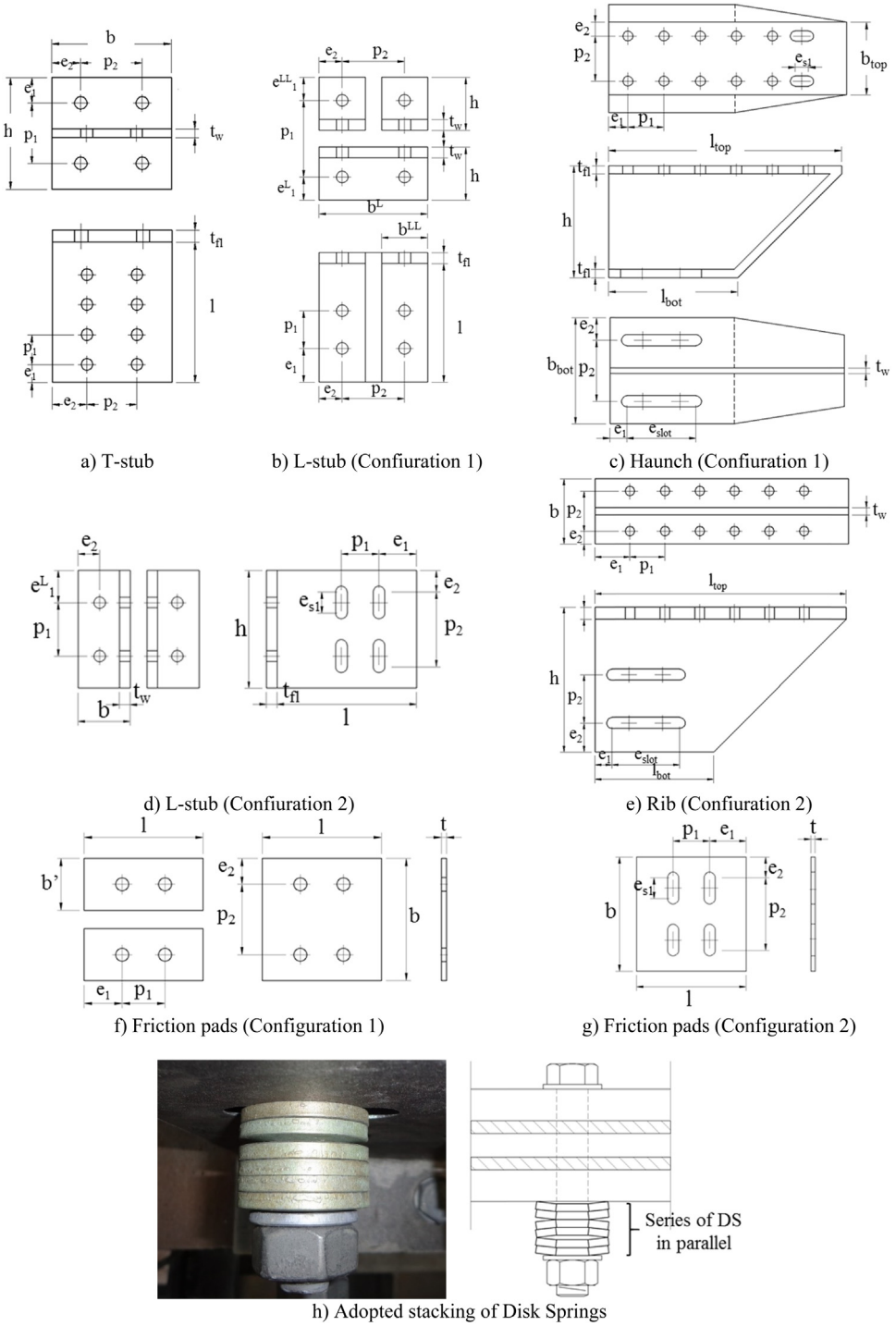


**Fig. 3.** Geometrical details of the tested friction devices.

**Table 1**
Specimen geometrical configuration.

| Specimen | Connection type | Beam | Column | Length of the Beam "L" *mm* | Length of the column "H" *mm* | Internal level arm of the connection "z" *Mm* | Thickness of beam web stiffener "$t_{stiff,\ beam}$" *mm* | Thickness of column continutiy plate "$t_{stiff,\ column}$" *mm* |
|---|---|---|---|---|---|---|---|---|
| **FD-1-1** | 1 | IPE270 | HE 220M | 1556 | 2700 | 478 | 10 | 10 |
| **FD -1-2** | 1 | IPE450 | HE 500B | 2906 | 2700 | 710 | 15 | 20 |
| **FD -2-1** | 2 | IPE270 | HE 220M | 1556 | 2700 | 458 | 10 | 10 |
| **FD -2-2** | 2 | IPE450 | HE 500B | 2906 | 2700 | 710 | 15 | 20 |

**Table 2**
T-stub geometry details.

| Specimen | Flange | | | | | | | | Web | | | | | | |
|---|---|---|---|---|---|---|---|---|---|---|---|---|---|---|---|
| | h mm | b mm | $t_{fl}$ mm | Bolts | $e_1$ mm | $p_1$ mm | $e_2$ mm | $p_2$ mm | l mm | $t_w$ mm | Bolts | $e_1$ mm | $p_1$ mm | $e_2$ mm | $p_2$ mm |
| **FD-1-1** | 187 | 200 | 20 | M20 | 43 | 101 | 48.3 | 103.4 | 235 | 15 | M18 | 30 | 50 | 58.3 | 83.4 |
| **FD-1-2** | 270 | 300 | 30 | M30 | 70 | 130 | 75 | 150 | 410 | 20 | M24 | 55 | 65 | 95.6 | 108.8 |
| **FD-2-1** | 195 | 200 | 20 | M20 | 45 | 105 | 38.3 | 123.4 | 260 | 15 | M18 | 30 | 50 | 58.3 | 83.4 |
| **FD-2-2** | 270 | 300 | 30 | M30 | 70 | 130 | 75 | 150 | 485 | 20 | M24 | 50 | 65 | 95.5 | 109 |

reduction of the connection bending capacity. The second feature directly affected the threshold and the evolution of flexural strength of the connection, because assuming larger clamping level (e.g. closer to the EC3 1-8 recommended value) corresponds to reduce the strength margin of the bolt shank as respect to the plastic damage, which can be anticipated at lower slip displacements of the device. Furthermore, the horizontal and vertical damper configurations induce different bearing forces on the clamped shank of bolts, which leads to different pattern of local plastic strain (see Fig. 13 in the Section 4.2) and strength degradation when the rotation demand increases.

The experimental tests showed negligible plastic deformation in the beam or the T and L-stubs up to 0.04 rad of chord rotation. Increasing the imposed rotation up to 0.05 rad (which was set as the limit of the allowable displacement capacity of the friction device) the overall response of the joints was still satisfactory, as shown in Fig. 9, without appreciable damage except for the unique case of FD-1-2-DS where the instability of the beam web occurred. This phenomenon occurred to activation of a strut transmission force between the theoretical center of rotation around the Tee web connecting the upper beam flange and the device, which has been better clarified by means of finite element simulation hereinafter (see Section 4.2). However, it is worth noting that this phenomenon can be influencing solely for deep beams and it can be easily prevented by using transverse web stiffeners at the tip of the beam.

After the tests, it was observed that the friction pads underwent significant erosion of the superficial friction coatings and signs of plastic deformation in the bolts were also spotted.

## 4. FEM

### 4.1. Modelling assumptions

The experimental tests were used to validate the finite element (FE) models developed using Abaqus v 6.14 [39]. The quasi-static analyses were performed by employing the Dynamic Implicit solver. The geometrical characteristics of the experimental assemblies were replicated in the FE software by modelling solid parts meshed using the C3D8R finite element (an 8-node linear brick with reduced integration). Both geometrical and mechanical nonlinearities were accounted for. The experimental tests on the large beam-to-column assemblies have suffered unexpected slippage in the connections between the column and the setup and therefore, the deformability source was taken into account in the numerical model. Fig. 10 depicts the general model shape

**Table 4**
Haunch geometry details.

| Specimen | $L_{top}$ mm | $L_{bot}$ mm | $t_{fl}$ mm | $t_w$ mm | Bolts | $e_1$ Mm | $p_1$ mm | $e_2$ mm | $p_2$ mm |
|---|---|---|---|---|---|---|---|---|---|
| **FD-1-1** | 419 | 234 | 15 | 10 | M18 | 35.5 | 67 | 25.8 | 83.4 |
| **FD-1-2** | 590 | 365 | 20 | 15 | M24 | 40.4 | 81 | 40.5 | 109 |
| **FD-2-1** | 520 | 245 | 15 | 15 | M20 | 72.1 | 72.1 | 25.8 | 83.4 |
| **FD-2-2** | 756 | 356 | 20 | 20 | M24 | 91.7 | 91.7 | 40.5 | 109 |

and the average material properties obtained experimentally.

The steel material properties were modelled based on the coupon tests performed in the laboratory as part of the experimental campaign, namely the yield stress was set equal to 380 MPa for beams, 427 MPa for columns and 443 MPa for both L-stub and T-stubs. The elastic modulus was assumed equal to 210,000 MPa and Poisson's coefficient equal to 0.3.

The nonlinear branch of the constitutive law was implemented using a half cycle input method and assuming both nonlinear kinematic and isotropic plastic hardening, as described by [30–33,40–42]. The bolts were modelled as shown by [43,44].

The model parts in contact, such as the bolts and plates, were assigned with interactions modelling both the Normal Behavior to avoid overclosure (by means of the “Hard Contact” option) and Tangential behavior to define the relative sliding (by employing the Coulomb friction law) [46]. In addition, to simulate the partial loss of the friction coefficient due to the smoothing of the superficial roughness of the friction pad, the temperature-dependent friction laws developed by the Authors [44] was used, thus friction coefficient decreases with the increase of temperature because of continuous sliding of plates. The reference friction properties are presented in Table 7. The simulations shown hereinafter were performed assuming the 5% dynamic percentile was used for the numerical simulations.

Since no plastic deformations are expected in the welded components, tie constraints linking together surfaces in contact have been used to replicate in a simplified manner the presence of full penetration welds.

The analyses were performed considering two loading steps: (i) bolt clamping and (ii) displacement history application.

The boundary conditions of the joints have been accurately simulated to reproduce those used during the tests. In addition, the beam was laterally restrained with out-of-plane restraints located in the same sections of the experimental setup. The AISC 341 [36] loading protocol

**Table 3**
L-stub geometry details.

| Specimen | Flange | | | | | | | | | Web | | | | | | |
|---|---|---|---|---|---|---|---|---|---|---|---|---|---|---|---|---|
| | h mm | $b^L$ mm | $b^{LL}$ mm | $t_{fl}$ mm | Bolts | $e_1{}^L$ mm | $e_1{}^{LL}$ mm | $e_2$ mm | $p_2$ mm | L mm | $t_w$ mm | Bolts | $e_1$ mm | $p_1$ mm | $e_2$ mm | $p_2$ mm |
| **FD-1-1** | 98 | 200 | 85 | 20 | M20 | 40 | 43 | 42.5 | 115 | 219 | 20 | M20 | 62 | 70 | 42.5 | 115 |
| **FD-1-2** | 145 | 300 | 135 | 30 | M30 | 60 | 60 | 67.5 | 165 | 360 | 30 | M20 | 85 | 70 | 67.5 | 165 |
| **FD-2-1** | 220 | 97.5 | | 20 | M20 | 60 | 100 | 40.5 | | 260 | 20 | M20 | 70 | 70 | 40 | 160 |
| **FD-2-2** | 330 | 132 | | 30 | M30 | 90 | 150 | 57 | | 366 | 30 | M20 | 83 | 70 | 65 | 200 |

**Table 5**
Friction pads geometry details.

| Specimen | l *mm* | b *mm* | b *mm* | t *mm* | Bolts | Disc spring | | $N_b$ *kN* | $e_1$ *mm* | $p_1$ *mm* | $e_2$ *mm* | $p_2$ *mm* |
|---|---|---|---|---|---|---|---|---|---|---|---|---|
| **FD-1-1** | 194 | 200 | 85 | 8 | M20 | w/ | w/o | 72 | 62 | 70 | 42.5 | 115 |
| **FD-1-2** | 310 | 300 | 135 | 8 | M20 | w/ | w/o | 87 | 85 | 70 | 67.5 | 165 |
| **FD-2-1** | 210 | 220 | | 8 | M20 | w/ | w/o | 78 | 70 | 70 | 40 | 160 |
| **FD-2-2** | 306 | 330 | | 8 | M20 | w/ | w/o | 96 | 83 | 70 | 65 | 200 |

up to 5% interstory drift ratio was applied at the beam end consistently with the test procedure.

### 4.2. Validations and discussion of results

The adopted modelling assumptions effectively simulate both the global and the local response of the tested joints, as it can be observed in Figs. 11 and 12 respectively. Since the transition from the static to the dynamic friction was not modelled, the response of the joint during the initial cycles are not accurately replicated. However, this inaccuracy disappears at increasing the number of cycles.

During the experimental campaign no damage was observed in the steel elements. However, the numerical analyses show some concentrations of slight plastic damage, depicted in terms of equivalent plastic strain (PEEQ) in Fig. 12, at the base of the web of the upper T-stub (where the center of rotation is located), and either at the bases of the L-stubs, at the top web-flange area of the beam underneath the T-stub and in the shear bolts of the device. Furthermore, plastic deformations can be observed in the shanks of the bolts in the friction device. Indeed, the horizontal damper configuration induces shear type bending effects in the shanks with two bearing contacts in all bolts of the device. On the contrary, the bolts in the vertical damper have one bearing zone at mid-length of the clamped shank, which leads to larger local plastic strain (see Fig. 13). In addition, in this second case the bolts close to the column face do not exhibit plastic strains.

A crucial aspect related to the design of the connections (T-stub and L-stub) at column face is the shear check, because these elements should guarantee the resistance due to combined tensile and shear forces to avoid premature failure. Fig. 14 shows the distribution of shear forces at the level of the Tee and L-stubs as well as the total shear force in the section at the column face. In both tested friction device configurations, the cumulated shear in the two components (i.e. the sum of the relevant absolute values) is larger than the overall shear force (see Fig. 14 a and c for type 1 and Fig. 14 b and d for type 2). In order to investigate the evolution of the shear force with the connection rotation, monotonic analyses under both hogging and sagging loading conditions were alternatively performed. The results presented in Fig. 15 confirm the previous observations and offer insight into the magnitude of the shear transferred by each component. Indeed, for the investigated cases, the L-stubs transfer larger shear force compared to the T-stub. Configuration 1 joints are characterized by levels of maximum shear force transferred by the Tee of about 50% of the total shear, while the L stubs reach values close to 100% of the total shear (Fig. 15 *a* and *c*). However, while Configuration 1 components transfer shear of up to maximum total shear, Configuration 2 assemblies (Fig. 15 *b* and *d*) exhibit the same behavior observed cyclically i.e. the shear in the components reach values larger than the total shear, with the shear transferred by the L-stubs reaching values almost 2 times larger than the total shear for rotation values close to 0.06 rad.

The differences of shear force distributions between the 2 components is mainly due to the larger stiffness provided by the L-stubs in the vertical plane and the vertical sliding force component. Indeed, the transfer mechanism of shear force amongst the components (see Fig. 16) is highly complex and configuration dependent. The type 1 joint (FD 1-1-DS) is characterized by same sign shear forces transferred by the L-stubs and in a smaller measure by the T-stub. On the contrary, the T-stub of FD 2-1-DS carries an opposite sign shear force, owing to the heightened level of shear force transferred by the L-stubs, in order to preserve the equilibrium at the column face. The hogging/sagging loading conditions lead to the same distribution of forces between the components for the same configuration, with a smoother transfer of the forces under positive bending.

In the analyses performed on the models depicting the experimental tests it was observed that small concentration of damage is located in the base of the T-stub, the L-stubs (in the case of Configuration 1), the bolts of the friction damper and in a reduced extent in the beam (the web-flange junction at the beam end immediately below the T-stub and in the slotted holes at the end of the beam-haunch connection). These

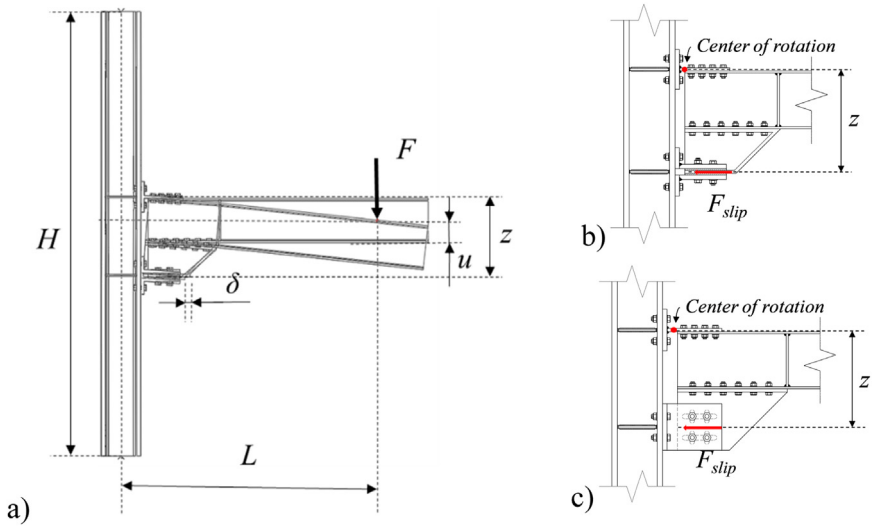


**Fig. 4.** Monitored parameters: global (a) and local response (b,c).

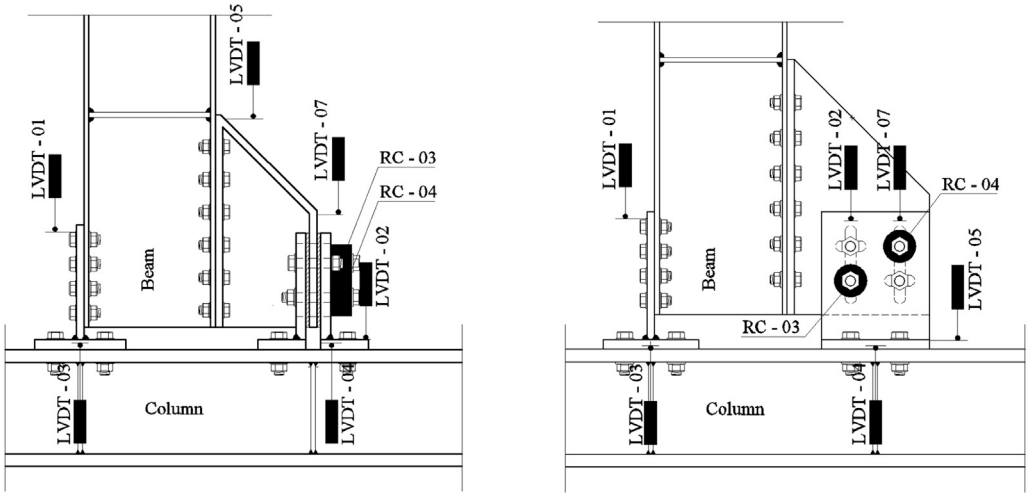


**Fig. 5.** Layout of displacement transducers to measure the local response of joints.

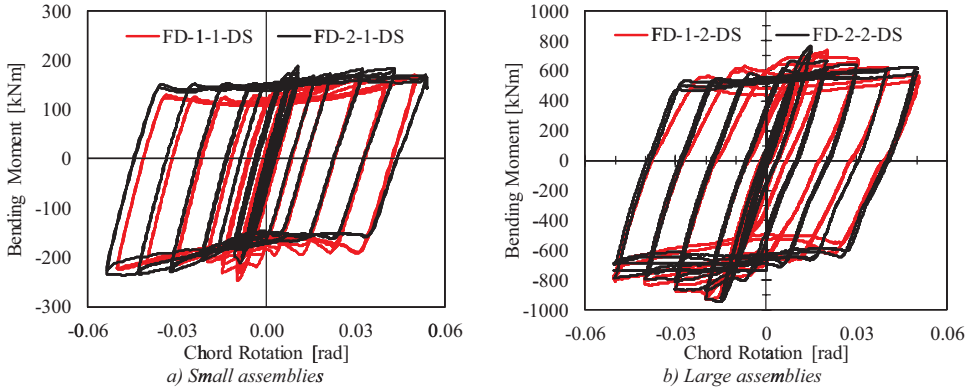


**Fig. 6.** Comparison between the response of the 2 device configurations.

results are presented in Fig. 17 in terms of PEEQ (equivalent plastic strain) distribution on the large beam to column assemblies. As it can be observed in the legend of PEEQ that are evaluated at the rotation equal to 0.05 rad, the horizontal friction damper configuration leads to larger plastic deformations in the joint elements. As a matter of fact, this result can also be observed in terms of dissipated energy, presented in Fig. 18. Indeed, the friction energy normalized with respect to the total dissipated energy for the first configuration is smaller compared to the second configuration and the opposite is true in terms of normalized plastic energy. Although the second damper configuration leads to

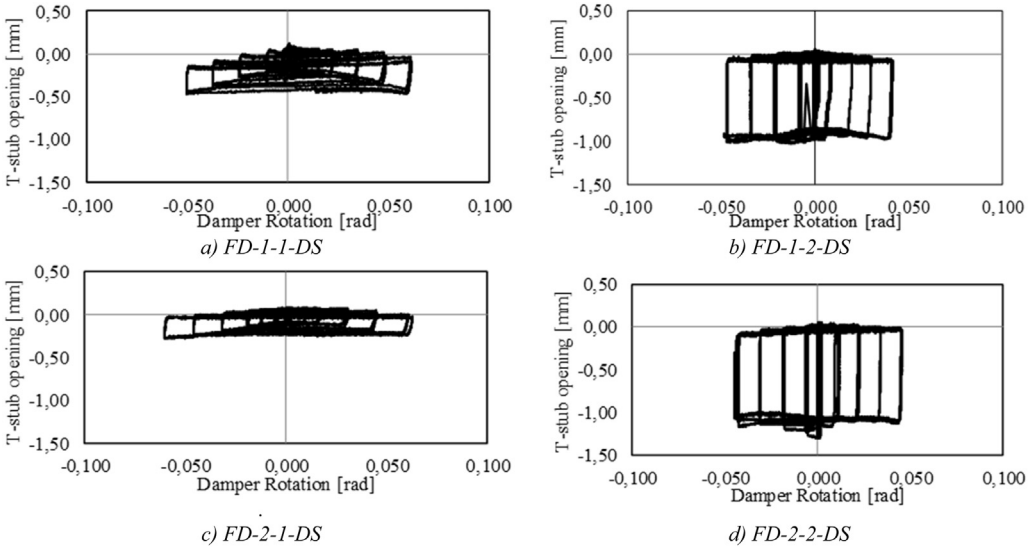


**Fig. 7.** T-stub opening versus damper rotation.

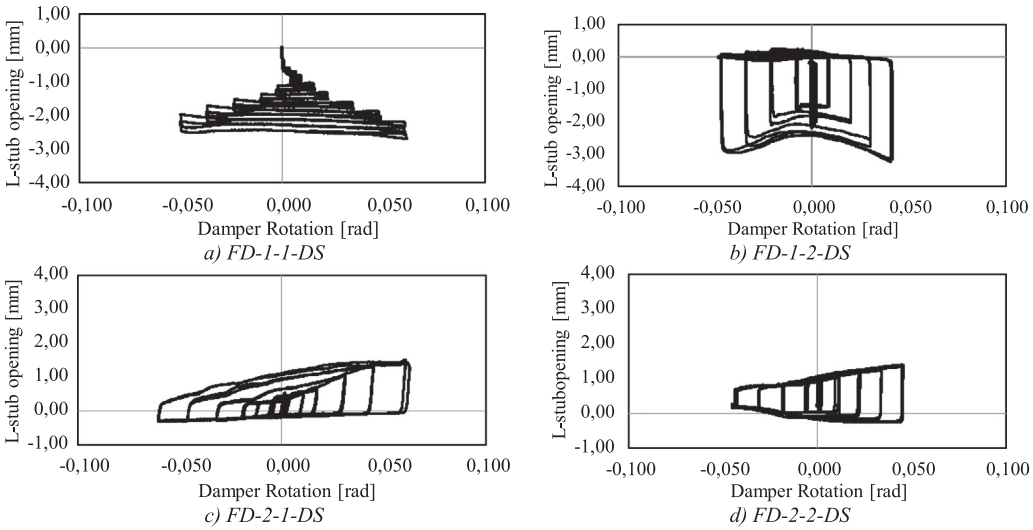


**Fig. 8.** L-stub opening versus damper rotation.

**Table 6**
Pretension levels in the bolts of the tested specimens.

| Model | $N_b$ [kN] | $N_b/F_{p,c}$ [%] |
|---|---|---|
| **FD-1-1** | 58 | 34% |
| **FD-1-2** | 98 | 57% |
| **FD-2-1** | 64 | 37% |
| **FD-2-2** | 105 | 61% |

lower plastic damage, it is worth noting that the plastic damage is limited for both configuration, maximum plastic energy dissipation is less than 5% of the total energy dissipated at 0.05 rad.

## 5. Parametric Fe analysis

### 5.1. Generality

The experimental tests confirmed the importance of the clamping force applied to the bolts into the device as well as the key role of the friction coefficient between the sliding surfaces. Therefore, the influence of the variation of these parameters on the response of the two tested joint configurations has been further investigated by means of finite element analyses based on the validated models described in Section 4. The examined parameters have been varied as follows:

- In addition to the pre-loading force adopted in the tests, namely $N_b$, a value 50% smaller (0.5 $N_b$) and a value 50% larger (1.5 $N_b$) have been considered. It should be noted that in all cases 1.5 $N_b$ is smaller than $F_{p,C}$ (which is equal to 172 kN for M20 gr.10.9 bolts).
- Three values of the dynamic friction coefficient $\mu$ are considered,

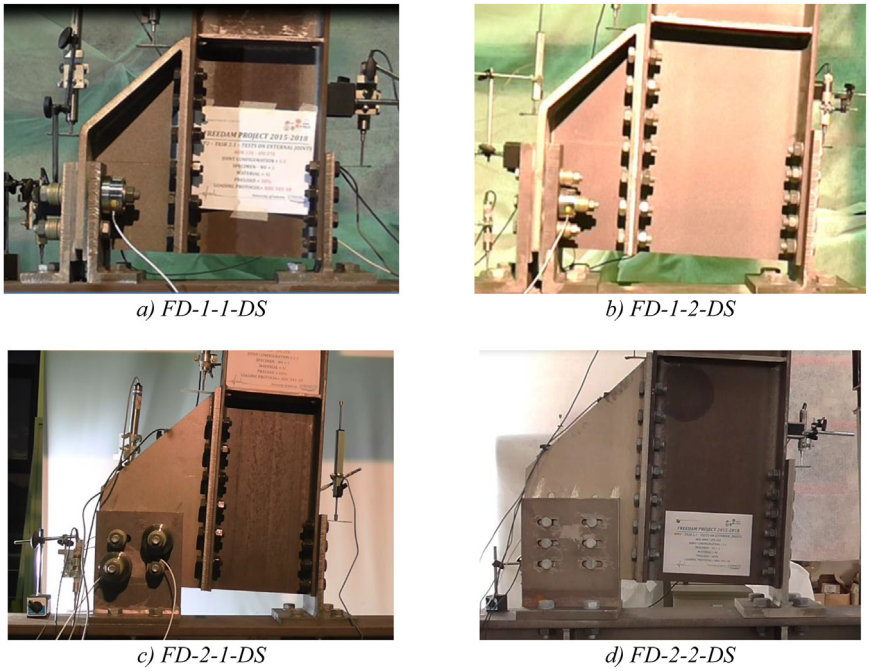


**Fig. 9.** Deformed shape of the tested specimens at chord rotation equal to 0.05 rad.

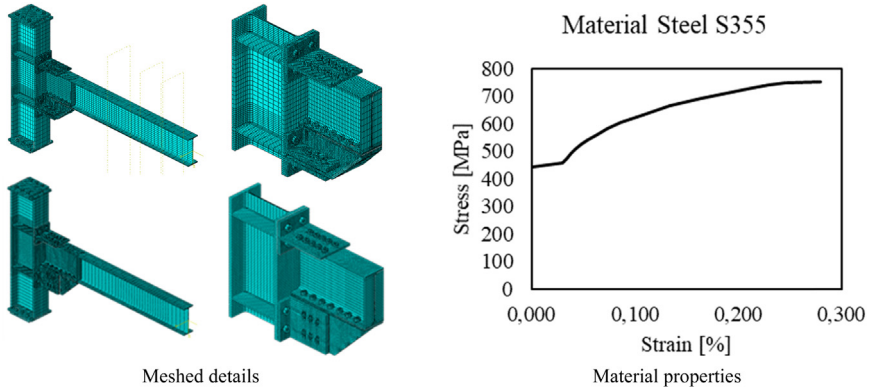


**Fig. 10.** Features of FE model.

**Table 7**
Friction material properties.

| Friction coefficient | *5% Percentile* $\mu_{5\%}$ | *95% Percentile* $\mu_{95\%}$ |
|---|---|---|
| Static | 0.69 | 0.84 |
| Dynamic | 0.53 | 0.65 |

namely the 5% percentile ($\mu_{5\%}$), see Table 6, the average value ($\mu_{avg}$) set equal to 0.59, and the 95% percentile ($\mu_{95\%}$), see Table 7.

### 5.2. Influence of clamping force

Fig. 19 shows the comparison of the response curves for the four joints (i.e. the two joint configurations and two assemblies) and Tables 8 and 9 report the numerically measured mechanical properties of the joints. The bending moments reported, $M^{(+)}$ and $M^{(-)}$, represent the bending moment at the occurrence of the sliding under sagging and hogging, respectively. Eqs. (6)–(8) clarify the meaning of the mechanical parameter reported in the tables.

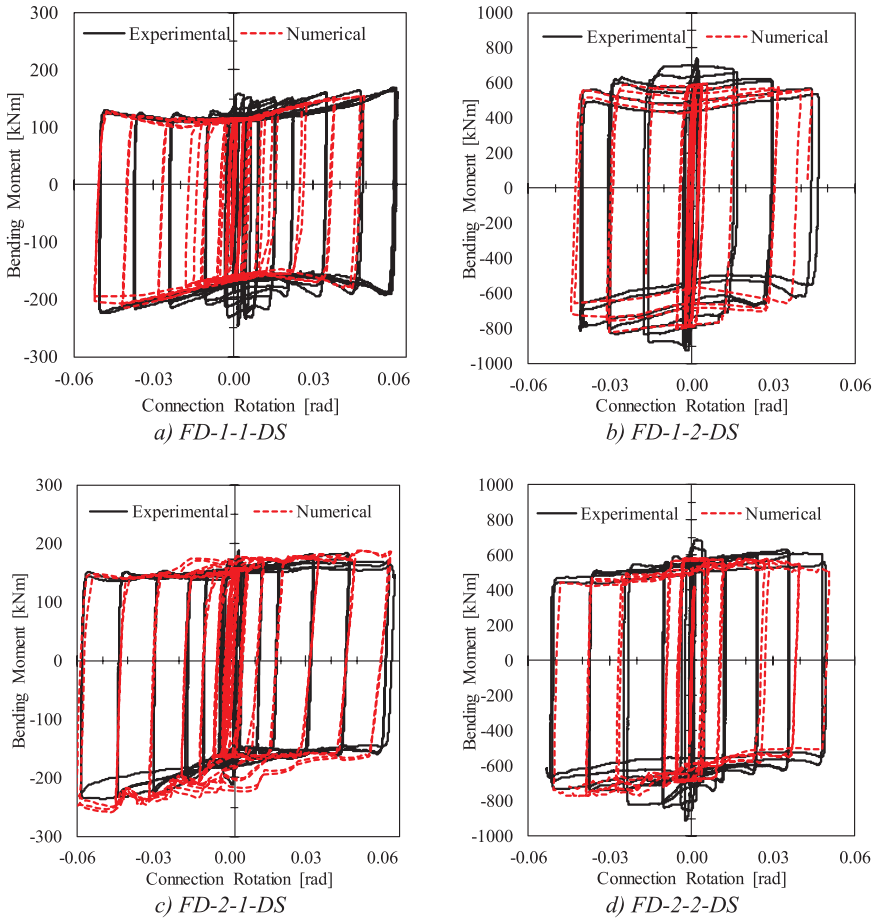


**Fig. 11.** Experimental vs numerical results in terms of Bending Moment – Connection rotation.

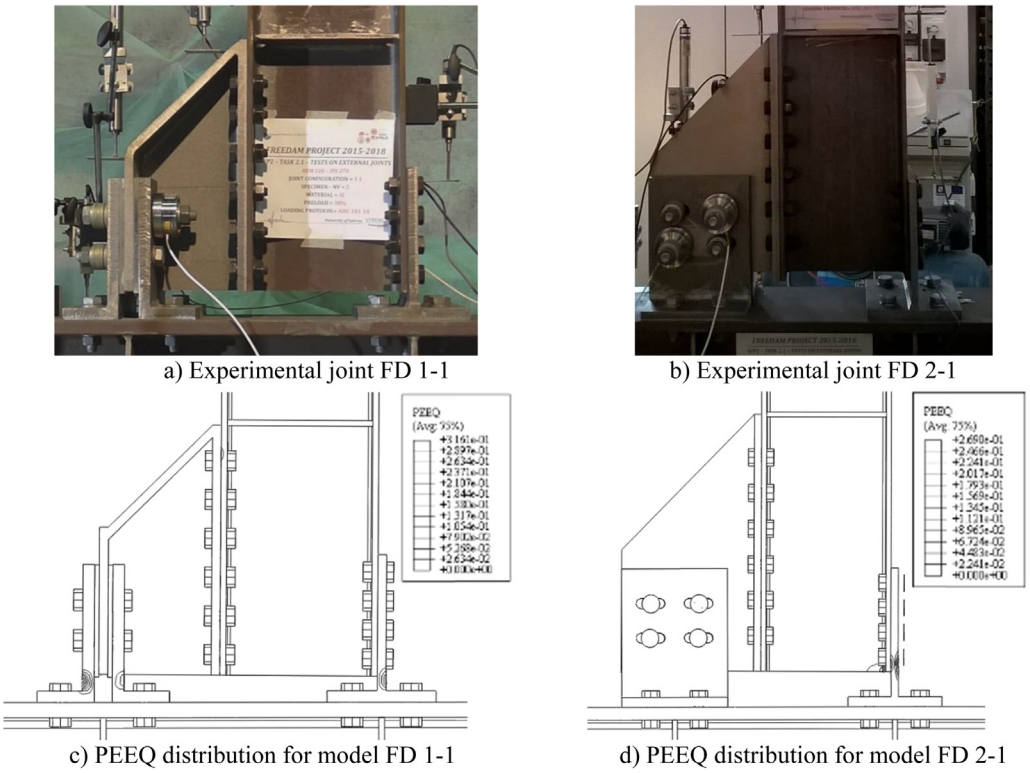


**Fig. 12.** Experimental vs. numerical models after cyclic test up to 5%.

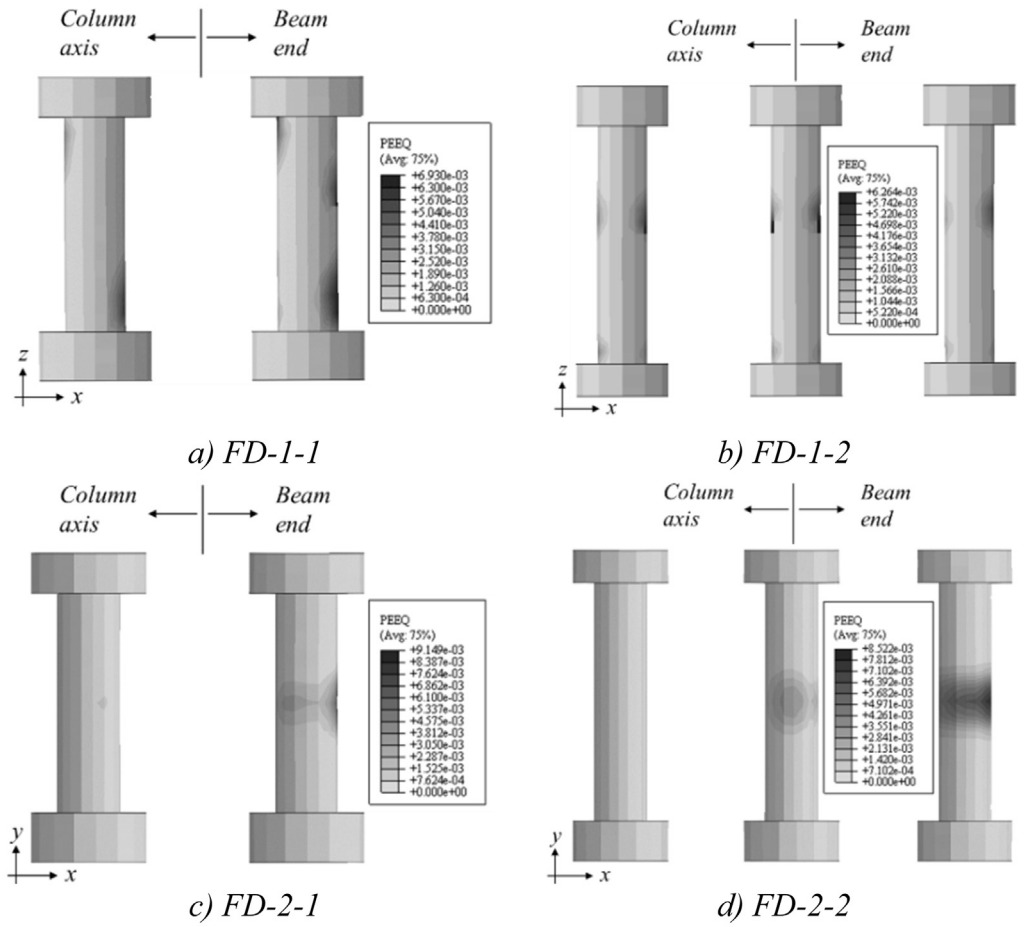


**Fig. 13.** Equivalent plastic damage (PEEQ) in the damper bolts.

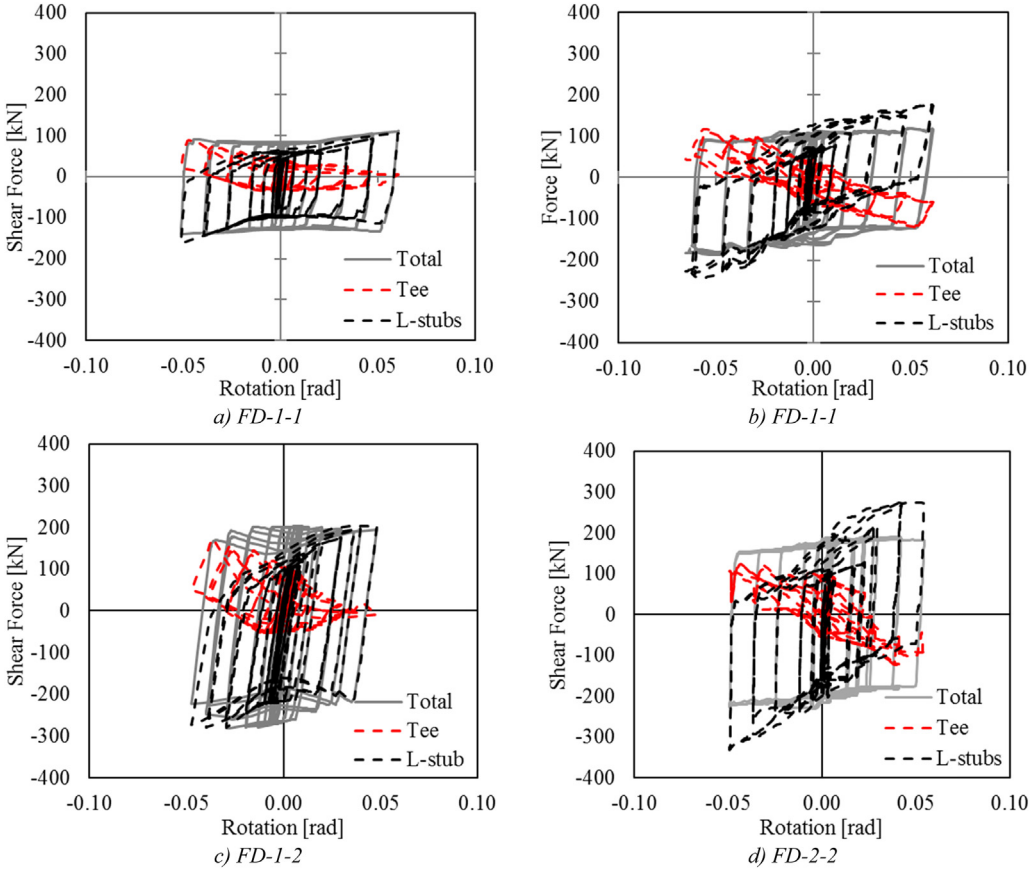


**Fig. 14.** Shear force transferred by different components.

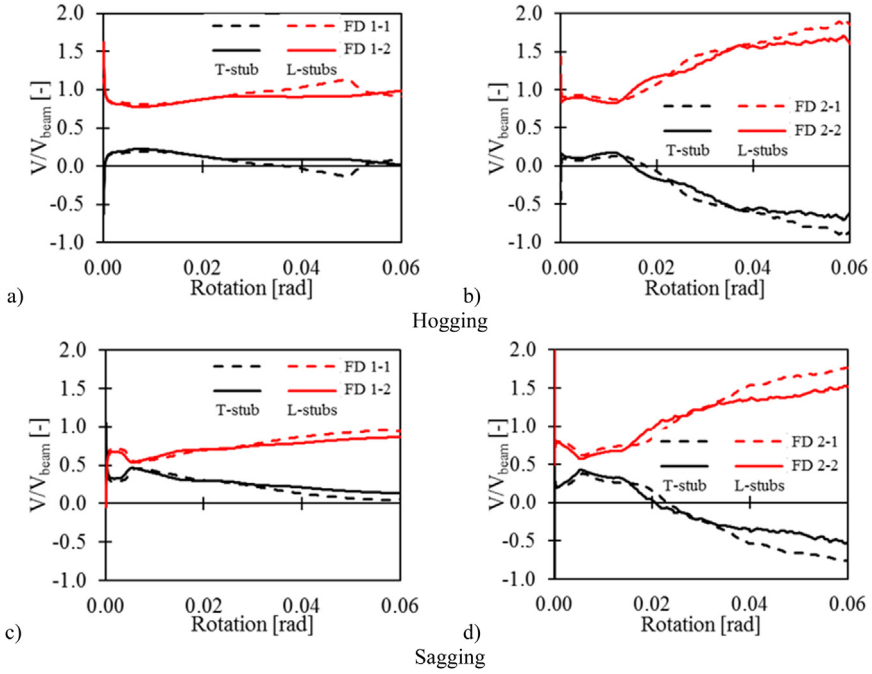


**Fig. 15.** Shear force at the connection face.

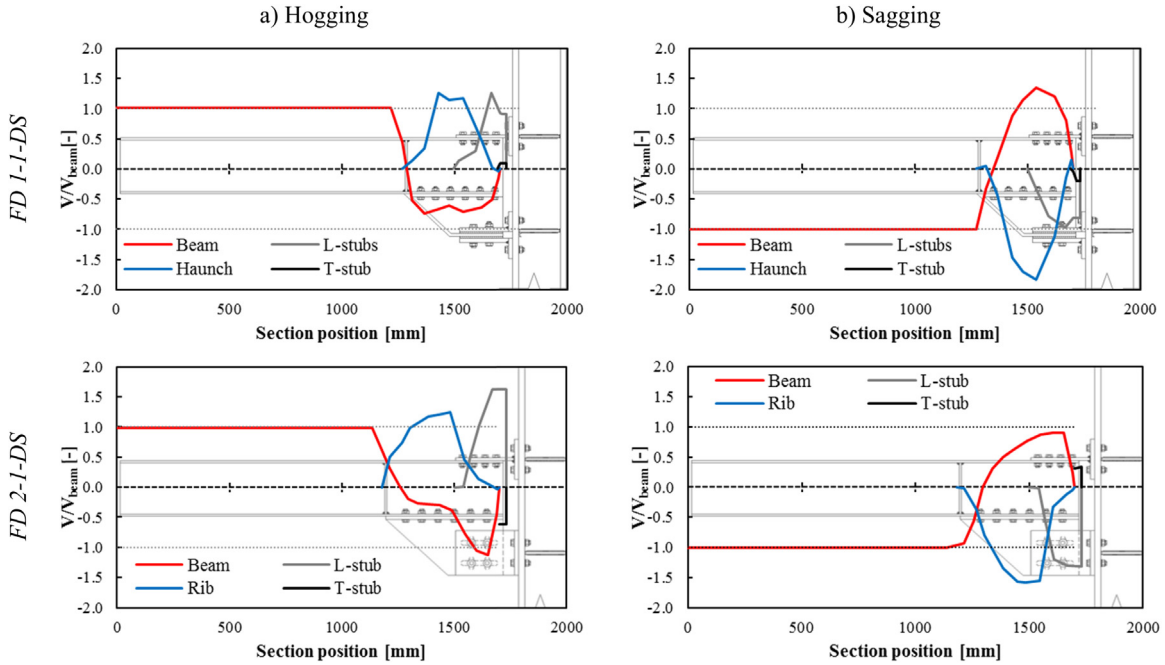


**Fig. 16.** Distribution of shear in the connected elements at 0.04 rad damper rotation.

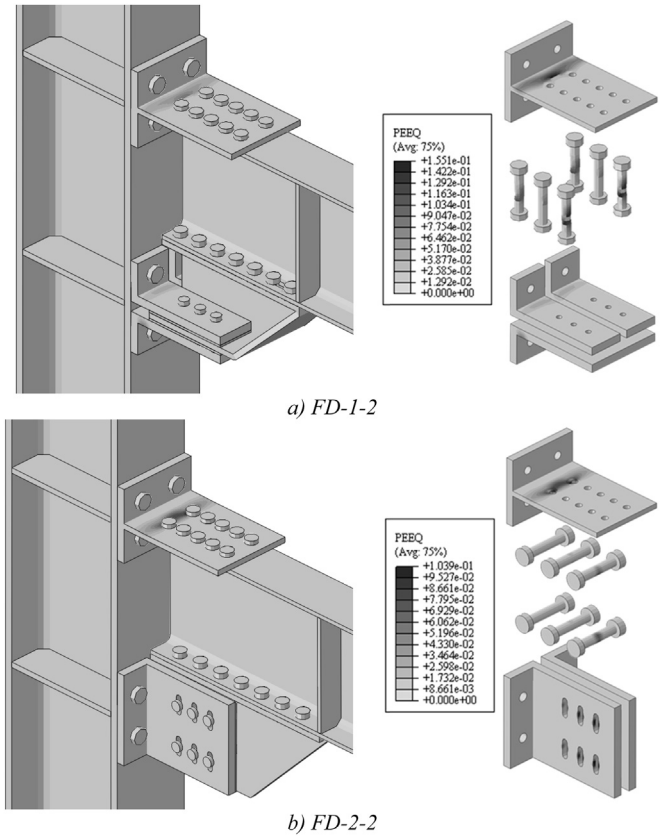


**Fig. 17.** PEEQ Distribution at the end of the cyclic analysis for large joint assemblies.

$$\Gamma^{(+)} = 1 + \frac{M^{(+)}_{0.5N_b} - M^{(+)}_{N_b}}{M^{(+)}_{N_b}} \quad (6)$$

$$\Gamma^{(-)} = 1 + \frac{M^{(-)}_{0.5N_b} - M^{(-)}_{N_b}}{M^{(-)}_{N_b}} \quad (7)$$

$$\Delta M^{(+/-)}/M^{(-)} = \frac{M^{(-)} - M^{(+)}}{M^{(-)}} \quad (8)$$

Where $\Gamma^{(+)}$ and $\Gamma^{(-)}$ represent the variation of the hogging and sagging bending moment capacity, respectively, considering alternatively the change in the clamping force from the design value $N_b$ to $0.5N_b$ and $1.5\,N_b$; $M^{(+)}$ and $M^{(-)}$ are the sagging and hogging bending moments. The subscripts depict the analysis from which the bending moment is taken, e.g. with clamping force equal to either $1.5\,N_b$ or $0.5\,N_b$; $\Delta M^{(+/-)}/M^{(-)}$ represents the difference between the hogging and sagging bending moment for each respective analysis (considering the three values for $N_b$).

As expected, the variation of the bending moment is proportional with the bolt pre-tension, although differently under both sagging and hogging. As reported in Tables 8 and 9, this difference is strictly related to the joint configuration and it is constant with the beam depths, clamping force, or friction coefficient. The difference is about 25% for Configuration 1% and 15% for configuration 2.

Further observation that can be made based on Fig. 19 is that the post-yield response of joint configuration 1 differs with the size of the beam-to-column assembly and with the level of preloading (relative to the maximum preloading force). In particular, the joint with shallow beam and lower relative preloading exhibits hardening (i.e. positive post-yield stiffness), while the joint with deeper beam and higher relative preloading shows softening (i.e. negative post-yield stiffness), the latter is more evident for the lower values of clamping force. These phenomena are more pronounced under hogging bending moment. The second configuration exhibits a more linear behavior in both examined assemblies.

The stiffness of the joint is not affected by the variation of clamping force, since it is determined by the stiffness of the other components of the joint (the connection at column face, the column web panel, etc.).

### 5.3. Influence of friction coefficient

Fig. 20 depicts the numerical curves in terms of bending moment vs.

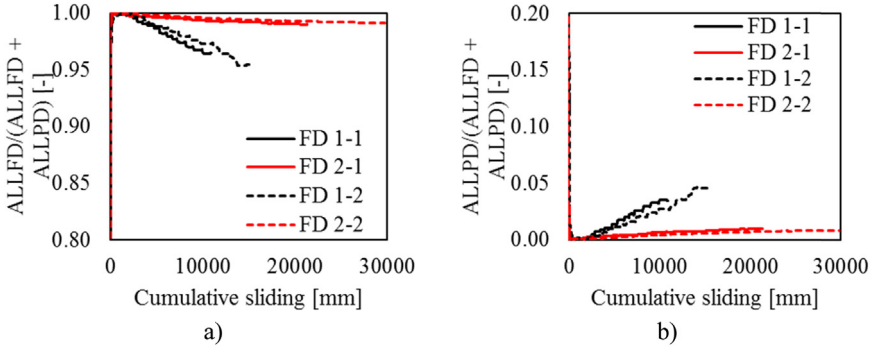


**Fig. 18.** Normalized disipated energy a) Friction energy and b) Plastic energy.

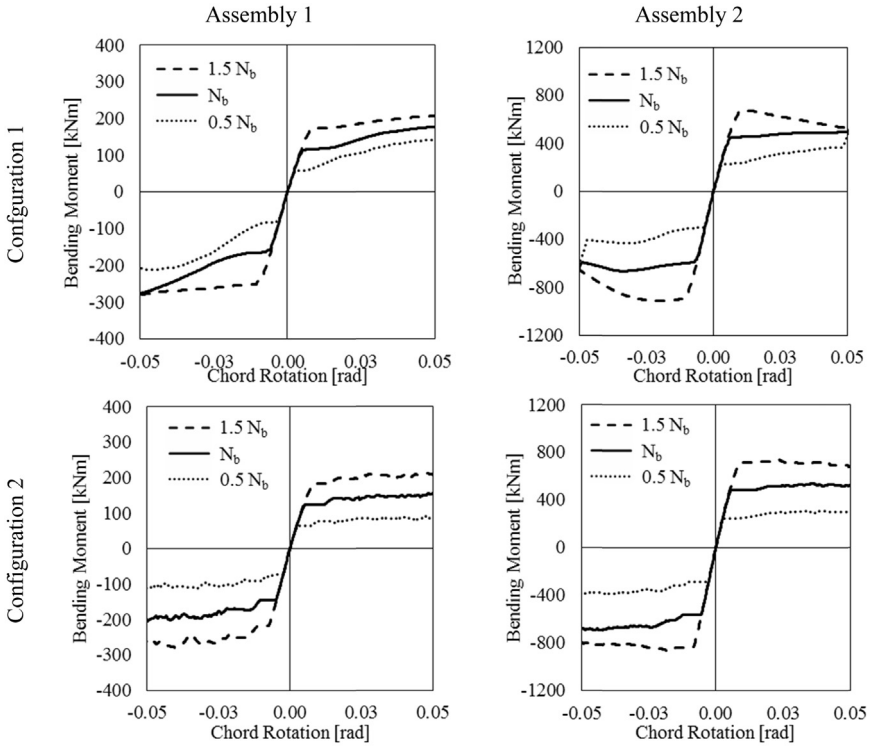


**Fig. 19.** Influence of the clamping force on the bending moment capacity.

**Table 8**
Bending moments for model FD 1–2-DS considering the variation of clamping force.

| Clamping force | $M^{(+)}$ [kNm] | $M^{(-)}$ [kNm] | $\Gamma^{(+)}$ [-] | $\Gamma^{(-)}$ [-] | $\Delta M^{(+/-)}/M^{(-)}$ [-] |
|---|---|---|---|---|---|
| $N_b$ | 453 | 602 | – | – | 25% |
| $0.5N_b$ | 230 | 298 | 51% | 50% | 23% |
| $1.5N_b$ | 690 | 902 | 152% | 150% | 24% |

**Table 9**
Bending moments for model FD 2-2-DS considering the variation of clamping force.

| Clamping force | $M^{(+)}$ [kNm] | $M^{(-)}$ [kNm] | $\Gamma^{(+)}$ [-] | $\Gamma^{(-)}$ [-] | $\Delta M^{(+/-)}/M^{(-)}$ [-] |
|---|---|---|---|---|---|
| $N_b$ | 484 | 564 | – | – | 14% |
| $0.5N_b$ | 250 | 290 | 52% | 51% | 14% |
| $1.5N_b$ | 714 | 838 | 148% | 149% | 15% |

chord rotation. It is possible to observe that the higher percentile of the friction coefficient values the larger is the joint capacity. This observation confirms the need to account for the variability of the friction properties of the friction pads to design the non-yielding structural members.

Similar hardening/softening behavior can be observed for both joint configuration and, additionally, the response curves seem scaled proportionality with the friction coefficient. Tables 10 and 11 depict the variation of the bending capacity of the FD-1-2-DS and FD-2-2-DS models analysed with larger values of friction coefficient ($\mu_{avg}$ and $\mu_{95\%}$) with respect to the design value ($\mu_{5\%}$) under hogging ($M^{(-)}$) and sagging ($M^{(+)}$) loading conditions. The variation in the case of FD-1–2-DS differs with respect to the variation of the friction coefficient. In particular, a larger increase of bending moment can be observed for the same increase of friction coefficient. On the other side, the analyses of model FD-2-2-DS in Table 11 show a closer dependency of the bending capacity with the friction property randomness.

The parameter $\Delta M^{(+/-)}/M^{(-)}$, evaluated also for this set of analyses confirms the previous observation regarding the relation between the damper's configuration and the different response under sagging and hogging conditions (values ranging around 25% for configuration 1%

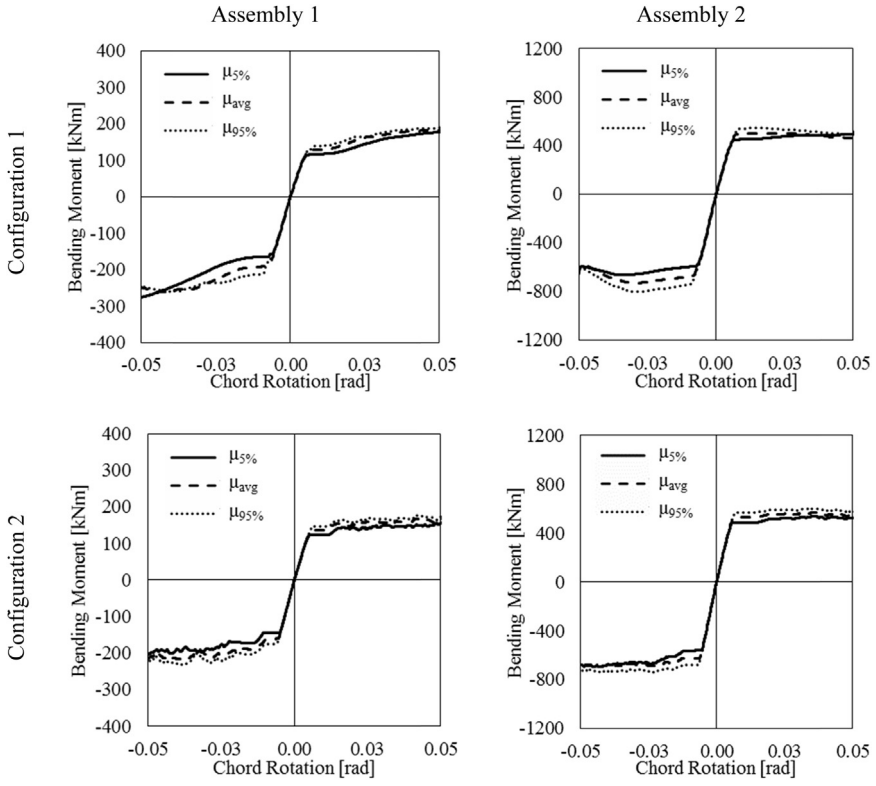


**Fig. 20.** The influence of the friction coefficient on the bending moment resistance.

**Table 10**
Bending moments for model FD 1-2 considering the friction coefficient variation.

| Friction coefficient | $\Delta\mu$ [-] | $M^{(+)}$ [kNm] | $M^{(-)}$ [kNm] | $\Gamma^{(+)}$ [-] | $\Gamma^{(-)}$ [-] | $\Delta M^{(+/-)}/M^{(-)}$ [-] |
|---|---|---|---|---|---|---|
| $\mu_{5\%}$ | – | 446 | 593 | – | – | 25% |
| $\mu_{avg}$ | 110% | 521 | 670 | 117% | 113% | 22% |
| $\mu_{95\%}$ | 117% | 535 | 733 | 120% | 124% | 27% |

**Table 11**
Bending moments for model FD 2-2 considering the friction coefficient variation.

| Friction coefficient | $\Delta\mu$ [-] | $M^{(+)}$ [kNm] | $M^{(-)}$ [kNm] | $\Gamma^{(+)}$ [-] | $\Gamma^{(-)}$ [-] | $\Delta M^{(+/-)}/M^{(-)}$ [-] |
|---|---|---|---|---|---|---|
| $\mu_{5\%}$ | – | 484 | 564 | – | – | 14% |
| $\mu_{avg}$ | 110% | 529 | 627 | 109% | 111% | 16% |
| $\mu_{95\%}$ | 117% | 568 | 679 | 117% | 120% | 16% |

and 15% for configuration 2).

## 6. Conclusive remarks

The seismic response of steel beam-to-column assemblies equipped with two types of friction dampers has been investigated by means of both experimental tests and finite element simulations. Based on the obtained outcomes, the following remarks can be drawn:

- Both types of friction joints provided satisfactory overall performance with stable and predictable hysteretic response, as well as preventing from damage the non-yielding members. However, non-symmetry response under sagging and hogging was observed.
- The joint configuration dictates the level of the response symmetry under sagging and hogging bending. The configuration with vertical friction surface exhibited slightly better response, showing lower degradation under cumulated rotation demand with smaller difference between hogging and sagging resistance. Indeed, the different resistance under sagging and hogging conditions ranges about 25% for the configuration with horizontal friction surface and 15% for that with vertical friction surface.
- The FE models accurately predict the response of experimental tests. The models allowed characterizing the local response of the joints, which exhibit some plastic deformations in the bolts and in the connecting L-stubs and T-Stubs. The FE analyses also showed that the joints equipped with the vertical friction damper exhibit plastic deformations lower than the corresponding device with horizontal friction surface.
- The variation of the bending capacity of both joint configurations is directly proportional with the bolt pretension force. Therefore, the bolt tightening process needs to be very well controlled because either larger or smaller tightening forces can impair the proper dissipative mechanisms. Indeed, the upper bound values lead to the development of larger forces in the damper, situation that hinders the hierarchy in the joint, while lower clamping forces can lead to sliding in the damper under serviceability conditions.
- The randomness of the friction properties has to be as much as possible mitigated and accounted for in the design phase, because this variability can inflict in the joint response and, consequently, the global behavior of the structure.

## Acknowledgements

The research activity herein presented has been supported by the European Union by research grant RFSR-CT-2015-00022. The support of the European Commission within RFCS Research & Innovation is gratefully acknowledged.

## References


[1] Bruneau M, McRae G. Reconstructing Christchurch: A Seismic Shift in Building Structural Systems. The Quake Centre, University of Canterbury; 2017.
[2] Christopoulos C, Filiatrault A. Principles of passive supplemental damping and seismic isolation. Pavia: IUSS PRESS; 2006.
[3] Soong TT, Spencer BF. Supplemental energy dissipation: state-of-the-art and state-of-the-practice. Eng Struct 2002;24:243–59.
[4] Mualla I, Belev B. Seismic response of steel frames equipped with a new friction damper device under earthquake excitation. Eng Struct 2002;24(3):365–71.
[5] Khoo H-H, Clifton C, Butterworth J, MacRae G, Fergurson G. Influence of steel shim hardness on the sliding hinge joint performance. J Constr Steel Res 2012;72:119–29.
[6] Khoo H-H, Clifton C, Butterworth J, MacRae G. Experimental study of full-scale self-centering sliding hinge joint connections with friction ring springs. J Earthq Eng 2013;17(7):972–97.
[7] Khoo H-H, Clifton C, MacRae G, Zhou H, Ramhormozian S. Proposed design models for the asymmetric friction connection. Earthquake Engng Struct. Dyn 2014.
[8] Yeung S, Zhou H, Khoo H-H, Clifton GC, MacRae GA. Sliding shear capacities of the asymmetric friction connection, 2013 NZSEE Conference, April 26–28, Wellington (Paper n. 27); 2013.
[9] Butterworth JW, Clifton GC. Performance of hierarchical friction dissipating joints in moment resisting steel frames. 12World Conference on Earthquake Engineering, Paper N. 718; 2000.
[10] Borzouie J, Macrae G, Chase J, et al. Cyclic performance of asymmetric friction connections with grade 10.9 bolts. Bridg Struct Eng 2015;45(1).
[11] Ono S, Nakahira K, Tsujioka S, Uno N. Energy absorption capacity of thermally sprayed aluminum friction dampers. J Therm Spray Technol 1996;5(3).
[12] Sato A, Kimura K, Suita K, Inoue K. Cyclic test of high strength steel beam-to-column connection composed with knee-brace damper and friction damper connected by high strength bolts. Proceedings of the SEEBUS 2009. Kyoto, Japan; 2009.
[13] Guneyisi EM, D'Aniello M, Landolfo R. Seismic upgrading of steel moment-resisting frames by means of friction devices. Open Constr Build Technol J 2014;8(Suppl 1: M9):289–99.
[14] Taghi Nikoukalam M,, Mirghaderi SR, Dolatshahi KM. Analytical study of moment-resisting frames retrofitted with shear slotted bolted connection. J. Struct. Eng 2015:04015019.
[15] Piluso V, Montuori R, Troisi M. Innovative structural details in MR-frames for free from damage structures". Mech Res Commun 2014;58:146–56.
[16] Latour M, Rizzano G, Santiago A, Simoes da Silva L. Experimental response of a low-yielding, re-centering, rocking base plate joint with friction dampers. Submitt Soil Dyn Earthq Eng 2018.
[17] Latour M, Piluso V, Rizzano G. Experimental analysis of innovative dissipative bolted double split tee beam-to-column connections. Steel Constr 2011;4(2).
[18] Latour M, Piluso V, Rizzano G. Free from damage beam-to-column joints: testing and design of DST connections with friction pads. Eng Struct 2015;85:219–33.
[19] Latour M, Piluso V, Rizzano G. Experimental analysis on friction materials for supplemental damping devices. Constr Build Mater 2014;65:159–76.
[20] Ferrante Cavallaro G, Francavilla A, Latour M, Piluso V, Rizzano G. Cyclic response of friction materials for low yielding connections. Submitt Soil Dyn Earthq Eng 2018.
[21] Ferrante Cavallaro G, Latour M, Francavilla AB, Piluso V, Rizzano G. Standardised friction damper bolt assemblies time-related relaxation and installed tension variability. J Constr Steel Res 2018;141:145–55.
[22] D'Aniello M, Zimbru M, Landolfo R, Latour M, Rizzano G, Piluso V. Finite element analyses on free from damage seismic resisting beam-to-column joints. Proceedings of COMPDYN 2017, Rhodes Island, Greece, 15–17 June; 2017.
[23] Latour M, Piluso V, Rizzano G. Experimental analysis of beam-to-column joints equipped with sprayed aluminum friction dampers. J Constr Steel Res 2018;146:33–48.
[24] Lemos A, da Silva LS, Latour M, Rizzano G. Numerical modelling of innovative DST steel joint under cyclic loading. Arch Civil Mech Eng 2018;18(3):687–701.
[25] CEN EN1993:1-8, Design of Steel Structures - Part 1-8: Design of Joints; 2005.
[26] CEN EN 1998-1, Design of structures for earthquake resistance - Part 1: General rules, seismic actions and rules for buildings; 2005.
[27] Faella C, Piluso V, Rizzano G. Structural steel semi-rigid connections. Boca Raton: CRC Press; 2000.
[28] Iannone F, Latour M, Piluso V, Rizzano G. Experimental analysis of bolted steel beam-to-column connections: component identification. J Earthq Eng 2011;15(2):214–44.
[29] Latour M, Piluso V, Rizzano G. Cyclic modeling of bolted beam-to-column connections: component approach. J Earthq Eng 2011;15:537–63.
[30] Cassiano D, D'Aniello M, Rebelo C. Parametric finite element analyses on flush end-plate joints under column removal. J Constr Steel Res 2017;137:77–92.
[31] Cassiano D, D'Aniello M, Rebelo C. Seismic behaviour of gravity load designed flush end-plate joints. Steel Compos Struct Int J 2018;26(5):621–34. https://doi.org/10.12989/scs.2018.26.5.621.
[32] D'Aniello M, Tartaglia R, Costanzo S, Landolfo R. Seismic design of extended stiffened end-plate joints in the framework of eurocodes. J Constr Steel Res 2017;128:512–27.
[33] Tartaglia R, D'Aniello M, Rassati GA, Swanson JA, Landolfo R. Full strength extended stiffened end-plate joints: aisc vs recent European design criteria. Eng Struct 2018;159:155–71.
[34] D'Aniello M, Tartaglia R, Costanzo S, Campanella G, Landolfo R, De Martino A. Experimental tests on extended stiffened end-plate joints within equal joints project. Key Eng Mater 2018;763:406–13. [ISSN: 1662-9795].
[35] Ferrante Cavallaro G, Francavilla AB, Latour M, Piluso V, Rizzano G. Experimental behaviour of innovative thermal spray coating materials for FREEDAM joints. Compos Part B: Eng 2017;115:289–99.
[36] ANSI/AISC 341-16. Seismic Provisions for Structural Steel Buildings. American Institute of Steel Construction; 2016.
[37] European Committee for Standardization (CEN), EN 14399-4 - High Strength Structural Bolting for Preloading - Part 3: System HV - Hexagon Bolt and Nut Assemblies; 2005.
[38] D'Aniello M, Zimbru M, Landolfo R, Latour M, Rizzano G, Piluso V. Finite element analyses on free from damage seismic resisting beam-to-column joints. Papadrakakis, M, Fragiadakis, M, editor. Proc of. COMPDYN 2017-16th ECCOMAS Thematic Conference on Computational Methods in Structural Dynamics and Earthquake Engineering - , Rhodes Island, Greece; 15–17 June 2017.
[39] Dassault, Abaqus 6.14 - Abaqus Analysis User's Manual, Dassault Systèmes Simulia Corp; 2014.
[40] Tartaglia R, D'Aniello M, Zimbru M, Landolfo R. Finite element simulations on the ultimate response of extended stiffened end-plate joints. Steel Compos Struct Int J 2018;27(6):727–45. https://doi.org/10.12989/scs.2018.27.6.727.
[41] Tartaglia R, D'Aniello M, Landolfo R. The influence of rib stiffeners on the response of extended end-plate joints. J Constr Steel Res 2018;148:669–90.
[42] Tartaglia R, D'Aniello M. Nonlinear performance of extended stiffened end plate bolted beam-to-column joints subjected to column removal. Open Civil Eng J 2017;11:369–83.
[43] D'Aniello M, Cassiano D, Landolfo R. Monotonic and cyclic inelastic tensile response of European preloadable GR10.9 bolt assemblies. J Constr Steel Res 2016;124:77–90.
[44] D'Aniello M, Cassiano D, Landolfo R. Simplified criteria for finite element modelling of European preloadable bolts. Steel Compos Struct Int J 2017;24(6):643–58.
[45] Zimbru M, D'Aniello M, De Martino A, Latour M, Rizzano G, Piluso V. Investigation on friction features of dissipative lap shear connections by means of experimental and numerical tests. Open Constr Build Technol J 2018;12(Suppl-1, M9):154–69.
[46] Francavilla AB, Latour M, Piluso V, Rizzano G. Simplified finite element analysis of bolted T-stub connection components. Eng Struct 2015;100:656–64.